Projections of Twenty-First-Century Climate Extremes for Alaska via Dynamical Downscaling and Quantile Mapping

RICK LADER

Department of Atmospheric Sciences, Geophysical Institute, and International Arctic Research Center, University of Alaska Fairbanks, Fairbanks, Alaska

JOHN E. WALSH

International Arctic Research Center, University of Alaska Fairbanks, Fairbanks, Alaska

UMA S. BHATT

Department of Atmospheric Sciences, Geophysical Institute, University of Alaska Fairbanks, Fairbanks, Alaska

PETER A. BIENIEK

International Arctic Research Center, University of Alaska Fairbanks, Fairbanks, Alaska

(Manuscript received 28 December 2016, in final form 5 July 2017)

ABSTRACT

Climate change is expected to alter the frequencies and intensities of at least some types of extreme events. Although Alaska is already experiencing an amplified response to climate change, studies of extreme event occurrences have lagged those for other regions. Forced migration due to coastal erosion, failing infrastructure on thawing permafrost, more severe wildfire seasons, altered ocean chemistry, and an ever-shrinking season for snow and ice are among the most devastating effects, many of which are related to extreme climate events. This study uses regional dynamical downscaling with the Weather Research and Forecasting (WRF) Model to investigate projected twenty-first-century changes of daily maximum temperature, minimum temperature, and precipitation over Alaska. The forcing data used for the downscaling simulations include the European Centre for Medium-Range Weather Forecasts (ECMWF) interim reanalysis (ERA-Interim; 1981–2010), Geophysical Fluid Dynamics Laboratory Climate Model, version 3 (GFDL CM3), historical (1976–2005), and GFDL CM3 representative concentration pathway 8.5 (RCP8.5; 2006–2100). Observed trends of temperature and sea ice coverage in the Arctic are large, and the present trajectory of global emissions makes a continuation of these trends plausible. The future scenario is bias adjusted using a quantile-mapping procedure. Results indicate an asymmetric warming of climate extremes; namely, cold extremes rise fastest, and the greatest changes occur in winter. Maximum 1- and 5-day precipitation amounts are projected to increase by 53% and 50%, which is larger than the corresponding increases for the contiguous United States. When compared with the historical period, the shifts in temperature and precipitation indicate unprecedented heat and rainfall across Alaska during this century.

1. Introduction

The effects of climate change and global warming on Alaska are unequivocal. From 1949 to 2012, the annual mean temperature increased 1.7°C and annual precipitation increased 3.1 mm; winter changes were most dramatic, with temperatures climbing 3.7°C and precipitation increasing by 7.2 mm (Bieniek et al. 2014). While the overall signal for warmer, wetter conditions is clear, there also exists substantial spatial variability across Alaska. The trend magnitude for temperature on the North Slope and the northern interior is consistently higher than the statewide average. For precipitation, interior locations show little to no trend, but much of southeast Alaska, while becoming wetter on an annual basis, shows significant drying during the spring months (Bieniek et al. 2014).

Arcticwide, the 12-month period from October 2015 through September 2016 was the warmest year on

Corresponding author: Rick Lader, rtladerjr@alaska.edu

DOI: 10.1175/JAMC-D-16-0415.1

record over the period 1900–2016 (Overland et al. 2016a). This broke the previous record set in 2007 that had been matched in 2011 and 2015 (Overland et al. 2016b). Heavy precipitation, defined as exceeding the 95th percentile of the distribution, increased by 18% across southern Alaska during the period from 1950 to 2002 (Groisman et al. 2005). Since 1979, the melt season for sea ice in the Arctic Ocean has lengthened by 37 days (Parkinson 2014); meanwhile, the lowest recorded maximum and minimum Arctic sea ice extents occurred in 2015 and 2012, respectively (U.S. Environmental Protection Agency 2016). The trend of Arctic sea ice extent is negative for all months, and the annual trend of loss, globally, is significant at the 99% confidence level (Parkinson 2014).

The Arctic is warming at twice the rate of the Northern Hemisphere because of positive feedback mechanisms in the climate system, often referred to as Arctic amplification (Bekryaev et al. 2010; Pithan and Mauritsen 2014). One mechanism for the amplification is the sea ice–albedo feedback, wherein reduced sea ice lowers the surface albedo of the ocean, thus enabling greater absorption of solar radiation and promoting further sea ice melt. Warming temperatures are also responsible for thawing permafrost, which leads to drier landscapes in regions of discontinuous permafrost and an increased wildfire threat. Ocean acidification, a response to the uptake of approximately one quarter of annual carbon dioxide emissions (Walsh et al. 2014), threatens biodiversity, commercial fisheries, and subsistence harvesting over the coastal waters of Alaska (Chapin et al. 2014). Increased river discharge and rapid glacial melt further exacerbate these problems by altering ocean chemistry.

Alaska is projected to experience major changes in extreme weather during the twenty-first century (IPCC 2012). Natural and human systems are adapted to the recently observed climate, but not necessarily for rare or unobserved conditions, so rapidly changing extreme weather patterns make these systems vulnerable to deterioration and destruction. To help understand how extreme events are changing globally, the Expert Team on Climate Change Detection and Indices (ETCCDI) developed a set of 27 indices (http://www.climdex.org/indices.html) that are based on the distributions of daily surface temperature and precipitation (Klein Tank et al. 2009). These include measures of absolute extremes (e.g., hottest and coldest days of the year), threshold exceedance (e.g., number of frost days), time duration (e.g., cold spells), and percentile-based extremes (e.g., heavy precipitation above the 95th percentile).

Sillmann et al. (2013a) used these indices to compare a 31-model ensemble from phase 5 of the Coupled Model Intercomparison Project (CMIP5) with reanalysis output and noted an observed pattern of asymmetric warming of extreme temperatures. That is, cold temperature extremes are rising faster than warm temperature extremes. Observed trends of extreme precipitation are also positive with greater spatial variability (Zhang et al. 2011). This is expected, given that rising temperatures increase the atmosphere's holding capacity for water vapor. While the global climate models generally replicate climate extremes, they also occasionally exhibit large errors owing to coarse resolution, particularly in mountainous regions.

Regional dynamical downscaling of the global models attempts to reduce these errors by providing gridded output at much finer spatial and temporal resolution. The Coordinated Regional Climate Downscaling Experiment (CORDEX; Giorgi et al. 2009), for example, includes an Arctic domain covering most of Alaska. The global models provide the initial and boundary conditions that are necessary for the regional models to run, as the atmospheric circulation output from regional models is heavily dependent on the forcing global model (Koenigk et al. 2015). The added value of dynamical downscaling will vary spatially and seasonally with the circulation regime.

For Alaska, Bieniek et al. (2016) downscaled the European Centre for Medium-Range Weather Forecasts (ECMWF) interim reanalysis (ERA-Interim; Dee et al. 2011) to 20-km spatial resolution using the Advanced Research core of the Weather Research and Forecasting (WRF) Model (Skamarock et al. 2008). Unlike many regional climate model simulations, the downscaling of historical conditions in this study was constrained by a reinitialization to a reanalysis (ERA-Interim) every 48 h. They found reduced biases in the downscaled products of monthly temperature and precipitation relative to the input reanalysis data when validated against the statistically downscaled dataset of Hill et al. (2015) and station observations. The improvement was especially apparent near coastlines and in areas of significant topography.

The utility of dynamical downscaling has been shown across Alaska for mass-balance modeling of the Gulkana Glacier (Zhang et al. 2007), studying extreme precipitation (Glisan and Gutowski 2014a,b), quantifying the fraction of attributable risk imposed by climate change to the 2015 Alaska fire season (Partain et al. 2016), and anticipating when the record-warm winter of 2015/16 could become normal (Walsh et al. 2017).

Future projections of extreme temperature and precipitation are dependent upon the expected radiative forcing from greenhouse gas emissions and aerosols. The CMIP5 prescribes four representative concentration pathways (RCPs) that provide a range of

radiative forcing between 2.6 and 8.5 W m^{-2} by the end of the twenty-first century (van Vuuren et al. 2011). Observed carbon dioxide emissions continue to closely track the highest forcing scenario, RCP8.5 (Peters et al. 2013). RCP8.5 assumes a global population increase to 12 billion by 2100 and notes a decoupling between legislation that is aimed to combat air or water pollution as opposed to strictly climate change policy (Riahi et al. 2011). In the Arctic, the observed trend of warming and rate of sea ice loss is even greater than projected by models forced by RCP8.5 [see Figs. 4 and 5 in Overland et al. (2014)].

Sillmann et al. (2013b) studied projected changes to the extremes indices with a multimodel ensemble from CMIP5 using several of the RCPs. For their Alaska region, they found a continued asymmetric warming, with cold extremes increasing more than warm ones. Under the RCP8.5 scenario, the annual minimum temperature is projected to climb 14.3°C by 2100 but the annual maximum only by 4.4°C; meanwhile, the annual maximum 5-day precipitation is projected to increase by an average of 16 mm statewide (Bennett and Walsh 2015). These studies also note that the greatest increases in extreme temperature and precipitation occur in winter for Alaska. During summer, the changes to extreme indices are often more comparable to lower latitudes. These studies of the CMIP5 models did not consider the biases or other systematic errors in the CMIP5 global models.

Alaska has a limited observational network, so reanalysis is often used as a gridded tool to assess climate model output (Lader et al. 2016). Therefore, to properly contextualize model projections, it is important to consider the bias of a climate model relative to reanalysis and also the bias of reanalysis relative to in situ observations. This leads to the following questions that this study addresses:

1) Does reanalysis compare more favorably to station observations than the historical climate model in terms of their long-term downscaled distributions?
2) Does dynamical downscaling reduce errors associated with extremes-relevant variables: daily maximum temperature T_{max}, minimum temperature T_{min}, and precipitation?
3) Under the RCP8.5 emissions scenario, how do downscaled projections of the climate extremes indices compare with previous studies that use coarser data?

2. Data and methods

This study incorporates the ERA-Interim from 1981 to 2010 (Dee et al. 2011) and two simulations from the Geophysical Fluid Dynamics Laboratory Climate Model, version 3 (GFDL CM3; Donner et al. 2011), from 1976 to 2100. All of these data have been dynamically downscaled with spectral nudging, providing hourly output across 49 vertical levels and 20-km spatial resolution as described in Bieniek et al. (2016). The choice of resolution was based on the decision to improve upon the widely used CORDEX data, which had 50-km spacing for its first phase, and for computational time efficiency. The WRF Model configuration includes the following physics options: microphysics (Morrison 2-moment; Morrison et al. 2009); radiation (Rapid Radiative Transfer Model; Iacono et al. 2008); cumulus (Grell 3D); planetary boundary layer (Mellor–Yamada–Janjić; Janjić 1994); surface layer (Monin–Obukhov); and land surface (Noah land surface model coupled with thermodynamic sea ice; Zhang and Zhang 2001). The two time frames spanned by the GFDL CM3 runs are a historical period from 1976 to 2005 and a future period (2006–2100) based on the RCP8.5 emissions scenario. The study domain covers eastern Russia, Alaska, much of northern Canada, and the adjoining oceans (Fig. 1).

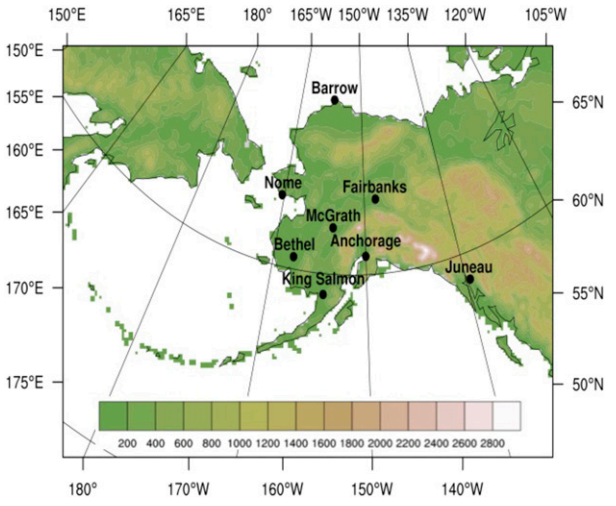

FIG. 1. Model topography (m) for downscaling domain with selected cities in Alaska.

The National Oceanic and Atmospheric Administration (NOAA) provides a visualization tool (http://www.esrl.noaa.gov/psd/ipcc/cmip5/) that enables users to compare each member of the CMIP5 with the ensemble means of temperature and precipitation. From 1979 to 2008, the GFDL CM3 agrees well with these ensemble means across Alaska. However, from 2006 to 2100, the GFDL CM3 projects a higher rate of warming that is nearly twice the CMIP5 ensemble mean for daily air temperature. It also projects a larger increase of precipitation across interior Alaska, with comparable changes over the southeast. Our choice of the GFDL

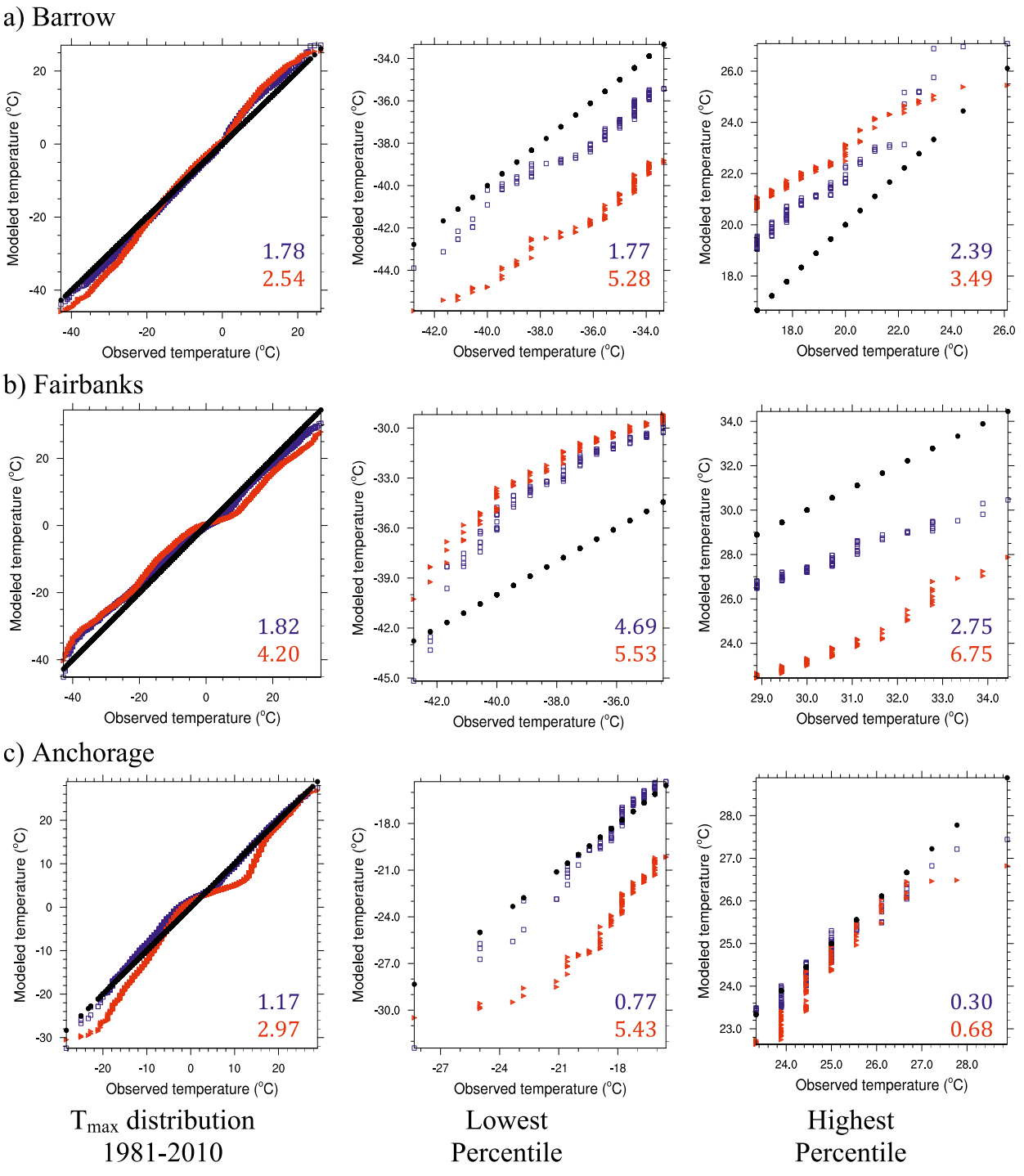

FIG. 2. The observed distribution of daily T_{max} (°C) from 1981 to 2010 (black) is compared with the nearest model grid cell of the downscaled ERA-Interim (blue), and GFDL CM3 (red) at (a) Barrow, (b) Fairbanks, and (c) Anchorage, Alaska. This includes the (left) full 30-yr distribution, (center) lowest percentile, and (right) highest percentile. The RMSE relative to observed is indicated in the bottom right of each plot.

CM3 model is motivated in part by the fact that Arctic warming and sea ice loss are occurring more rapidly than in most CMIP5 simulations (Overland et al. 2014). Laliberté et al. (2016) showed that the GFDL CM3 is one of the top-performing CMIP5 models for capturing the summer sea ice concentration when compared with a recent decade of passive microwave imagery. Walsh et al. (2017, manuscript submitted to *Environ. Modell.*

Software) show that GFDL CM3 ranks third among 21 CMIP5 models in the simulation of the seasonal cycles of temperature, precipitation, and sea level pressure over Alaska. Finally, as shown in section 4, indices of extremes based on GFDL CM3 are generally in the midrange of the indices based on other CMIP5 models.

A major contribution of this study is the hybrid dynamical downscaling and quantile-mapping approach used to investigate projected changes to extreme climate for Alaska. Dynamical downscaling of the GFDL CM3 from 2° latitude × 2.5° longitude to 20 km × 20 km is here shown to provide value-added information, particularly for temperature. The subsequent application of a quantile-delta mapping algorithm serves to bias adjust the GFDL CM3 RCP8.5 scenario using the observation-based ERA-Interim.

Quantile approaches of statistical downscaling are generally superior to a simple delta method because each point in the distribution gets a unique adjustment (Hayhoe 2010). These incorporate changes to the mean and variance rather than only to the mean. However, the quantile-mapped data are also tied to the relationships between large-scale features and the climate inherent to the reanalysis, which are assumed to remain stationary.

A quantile-delta mapping algorithm (Cannon et al. 2015) was employed to bias adjust the downscaled GFDL CM3 RCP8.5 projections. This takes the relative change at each point in the distribution of the GFDL CM3 between the projection and the historical period and applies it to the ERA-Interim, which acts as an observational dataset. This is described mathematically as follows:

$$x(t) = F_R^{-1}[q(t)] \times \frac{F_P^{-1}[q(t)]}{F_H^{-1}[q(t)]}, \quad (1)$$

where $x(t)$ represents the corrected value and $F^{-1}[q(t)]$ represents the quantile functions of the observed ERA-Interim R, future GFDL CM3 RCP8.5 projection P, and the historical GFDL CM3 simulation H. More generally, the quantile function is defined as

$$F^{-1}[q(t)] = \min\{x \in \mathbb{R}: F(x) \geq q(t)\},\ q(t) \in \{0,1\}, \quad (2)$$

where $F(x)$ is the cumulative distribution function of the variables, in this case, temperature and precipitation, and $\mathbb{R}$ denotes the set of real numbers. For example, the 90th-percentile precipitation of the future projected distribution is divided by the 90th-percentile precipitation from the GFDL CM3 historical simulation to obtain a modeled ratio of change. This ratio is then multiplied by the 90th-percentile precipitation of the observed reanalysis distribution to obtain a bias-adjusted future projection. The percentile values, and all other points, are obtained via the quantile function [(2)]. The same procedure is applied to temperature. For precipitation values that are less than 1, the modeled change is calculated by subtraction, and this delta is then added to the observed reanalysis value.

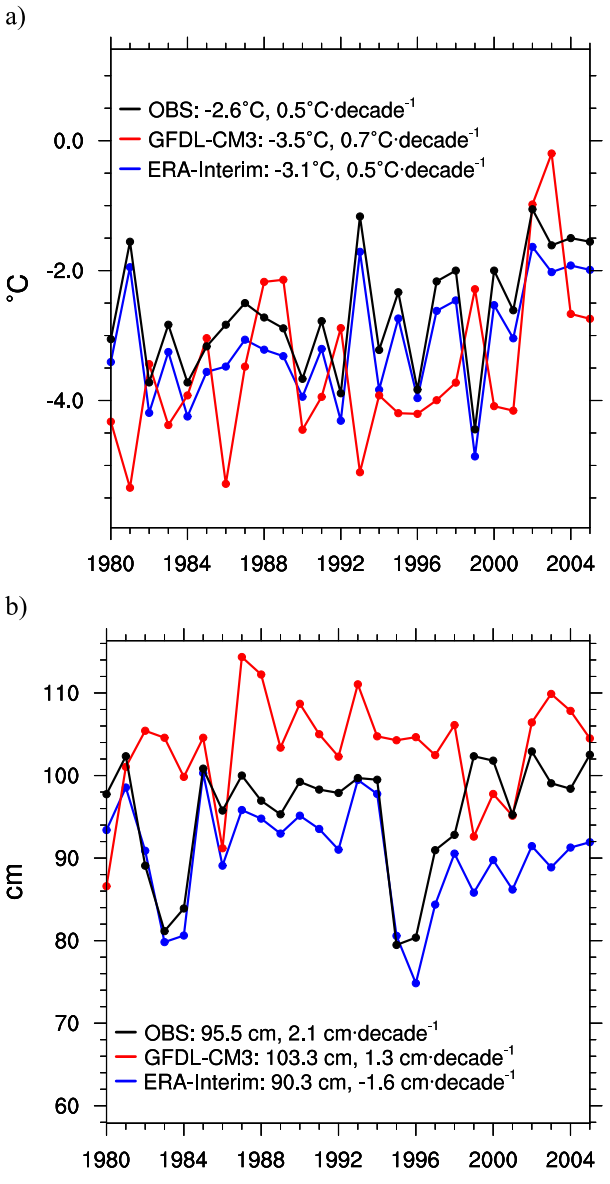

FIG. 3. Average annual statewide (a) temperature and (b) precipitation for observations (black), ERA-Interim (blue), and GFDL CM3 (red) from 1980 to 2005. The historical mean and linear trend for each time series are indicated.

The procedure works with successive 30-yr periods so that bias-adjusted data are produced from 2011 to 2040, 2041 to 2070, and 2071 to 2100, using 1981–2010 as the reanalysis baseline. The period from 1976 to 2005 is the historical period used for the GFDL CM3 because

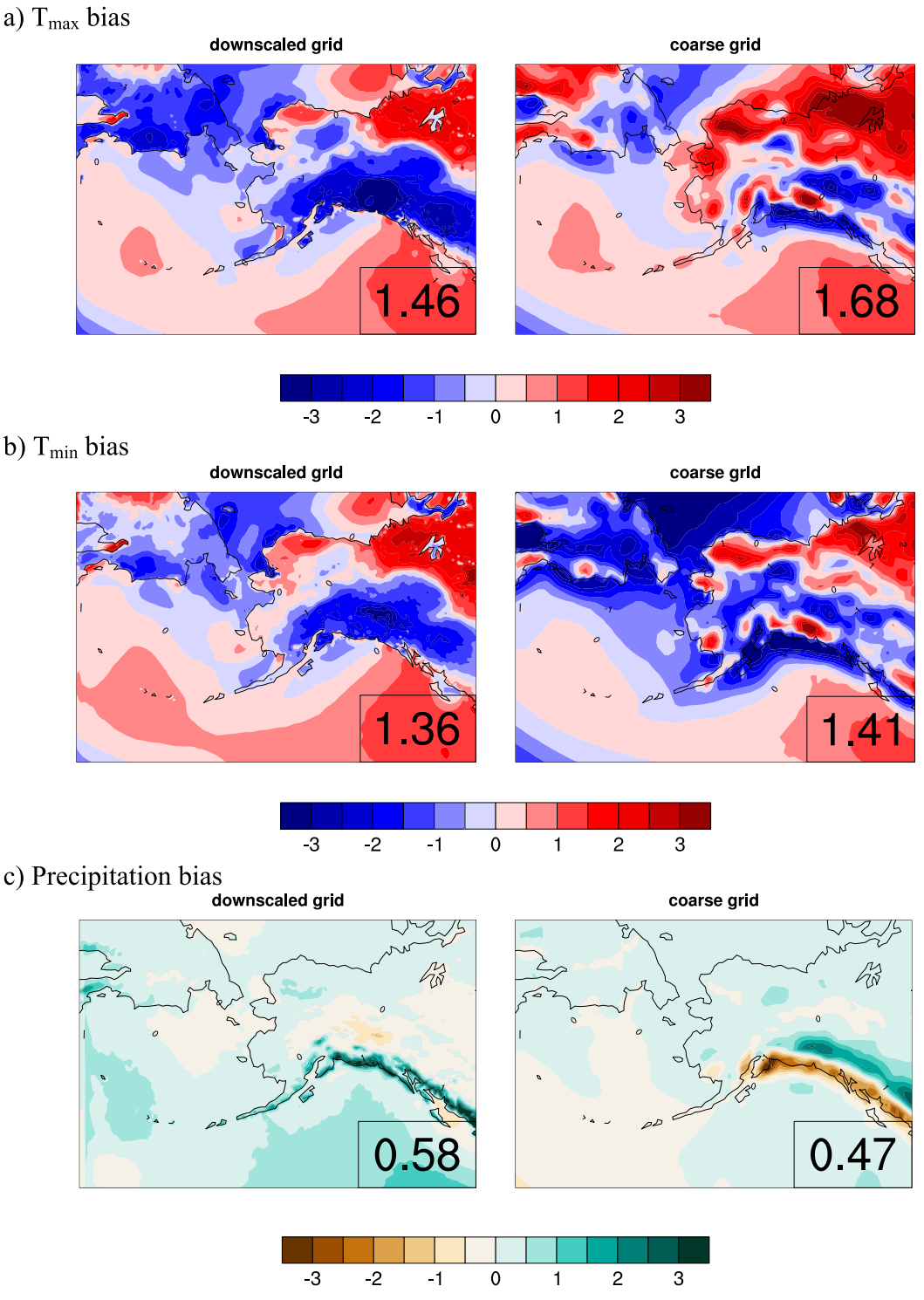

FIG. 4. RMSE (GFDL CM3 minus ERA-Interim) of daily (a) T_{max} (°C), (b) T_{min} (°C), and (c) precipitation (mm) from 1981 to 2005 for the (left) downscaled and (right) coarse domains. The gridpoint average RMSE is shown at the bottom right.

TABLE 1. Statewide average of climate extremes indices for 30-yr periods, including ID, SU, GSL, FD, TR, R10, R20, RX1, RX5, CWD, and CDD. The values represent annually averaged counts or magnitudes. GSL represents the period beginning on the sixth consecutive day with a daily mean temperature above 5°C in spring and ends on the sixth consecutive day below 5°C in autumn. The percent change marks the relative difference between 2071–2100 and 1981–2010. Signal emergence denotes when the 10-yr running mean anomaly continuously exceeds $\pm 2\sigma$ relative to the historical distribution.

Index	Threshold (if applicable)	Units	1981–2010	2011–40	2041–70	2071–2100	Percent change	Signal emergence
ID	$T_{max} < 0$°C	days	165.4	148.7	126.2	102.4	−38.1	2038
SU	$T_{max} > 25$°C	days	1.5	4.6	13.2	29.7	1880.0	2036
GSL	—	days	114.5	130.8	148.2	163.4	42.7	2035
FD	$T_{min} < 0$°C	days	219.2	197.0	171.3	148.1	−32.4	2026
TR	$T_{min} > 20$°C	days	0.0	0.1	1.2	6.8	—	2058
R10	$P \geq 10$ mm	days	22.8	26.8	32.4	37.8	65.8	2026
R20	$P \geq 20$ mm	days	6.7	8.3	10.6	13.5	101.5	2026
RX1	—	mm	34.4	39.5	45.9	52.7	53.2	2026
RX5	—	mm	71.0	81.0	93.5	106.4	49.9	2043
CWD	—	days	9.9	10.6	11.5	12.2	23.2	None
CDD	—	days	22.9	21.0	19.4	18.2	−20.5	None

the simulation ends in 2005, but this difference should not have a significant effect on the final products. Also note that the quantile-delta algorithm is applied locally, (i.e., at each grid box) to best preserve modeled changes.

This bias adjustment using reanalysis is justified because the ERA-Interim consistently has a lower root-mean-square error (RMSE), in terms of statistical distribution, when compared with station observations, than the historical GFDL CM3 does. This is also true when

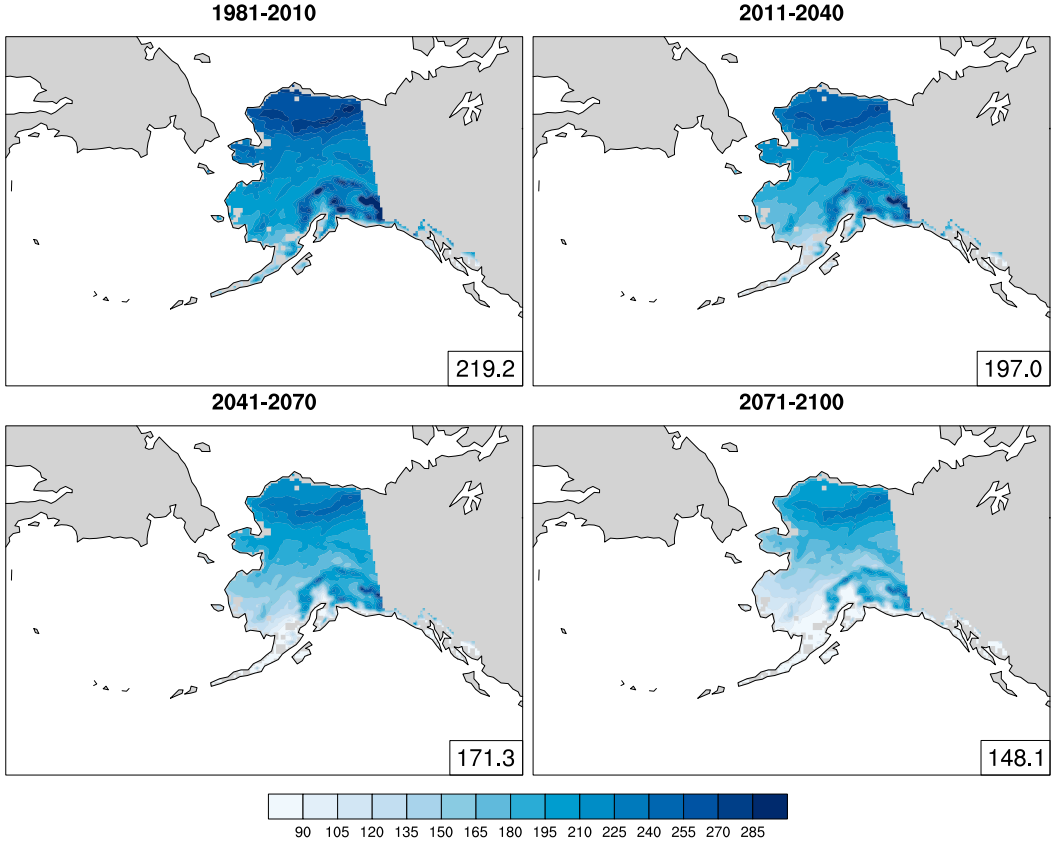

FIG. 5. Number of FD ($T_{min} < 0$°C) per year averaged for successive 30-yr periods. The statewide average is located at the bottom right.

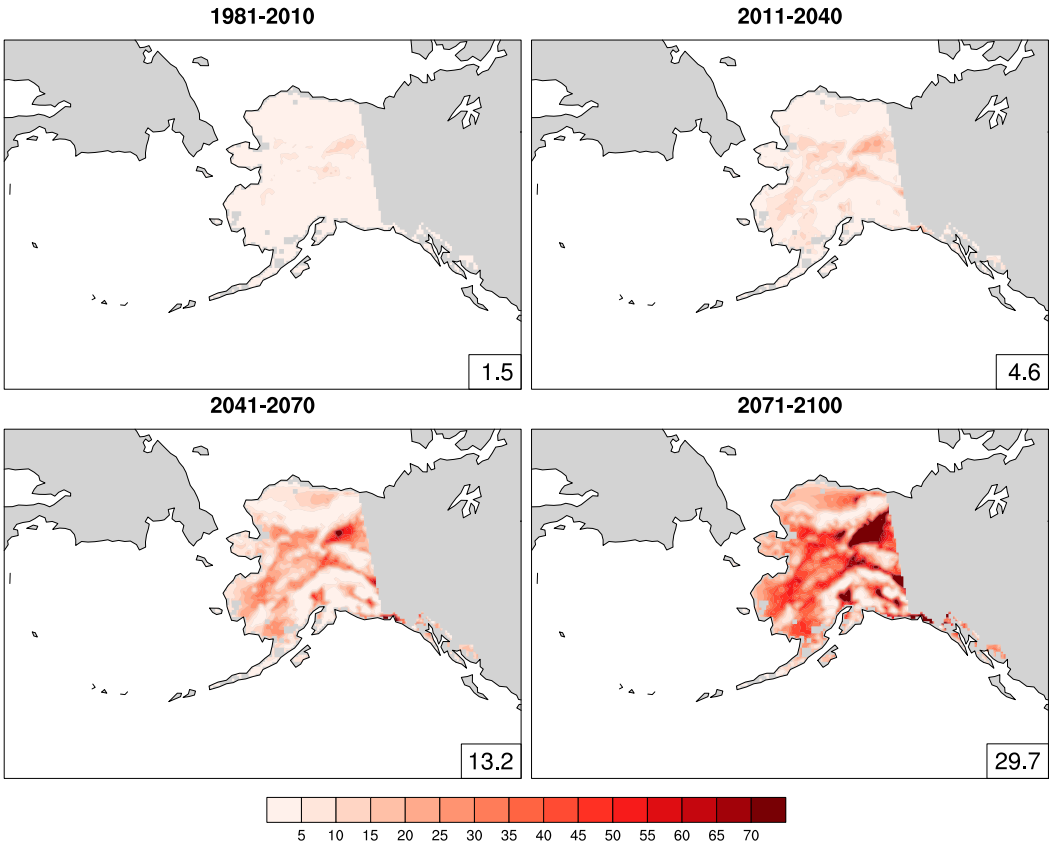

FIG. 6. As in Fig. 5, but for SU ($T_{max} > 25°C$).

restricting the sample to the highest and lowest percentiles, which is relevant for extreme events. Figure 2 shows this result for daily T_{max}; findings for daily T_{min} and precipitation are similar. The closer correspondence of the station data to ERA-Interim when compared with GFDL CM3 is expected because ERA-Interim assimilates station and satellite observations, whereas the GFDL CM3 does not. Consider also that the model grid cells used for each station have the same elevation because both downscaling simulations were conducted using WRF.

For the overlapping period of 1980–2005, the annual mean statewide ERA-Interim temperature (−3.1°C) compares more favorably to observations (−2.6°C) than does the GFDL CM3 (−3.5°C). Figure 3a shows the corresponding time series. Similarly, for precipitation, ERA-Interim (90.3 cm) is closer to observed (95.5 cm) than is the GFDL CM3 (103.3 cm; Fig. 3b). The observations are from NOAA's "climate at a glance" tool (available at http://www.ncdc.noaa.gov/cag/; NCEI 2017). The quantile-delta mapping procedure temporarily removes the date associated with any particular value and sorts the respective distributions in ascending order. The date is kept track of, however, so that the correct ratio can be applied to the correct point in the reanalysis distribution, thus producing the projected time series. In this way, the projected data reflect changes to the 30-yr distribution more than they do to the trend.

Another test compares the spatially averaged RMSE of the coarse-scale forcing data with their downscaled products. If ERA-Interim is considered "truth," both before and especially after downscaling, as previous studies already mentioned suggest, are the errors larger or smaller when comparing the coarse and downscaled GFDL CM3 datasets with their reanalysis counterparts? Figure 4 shows that the RMSE of daily T_{max} and T_{min} for a 25-yr climatology from 1981 to 2005 are lower in the downscaled GFDL CM3. This is true for the entire study domain and when only comparing grid cells over land. For precipitation, the coarse GFDL has a lower RMSE when averaging over the entire domain, but the values are equal over land. These results indicate that dynamical downscaling, which provides an improved representation of topography, reduces climate model errors for land areas. Along the coastal mountains of southern Alaska, the sign of the model precipitation bias changes from being too dry prior to downscaling to then too wet after downscaling.

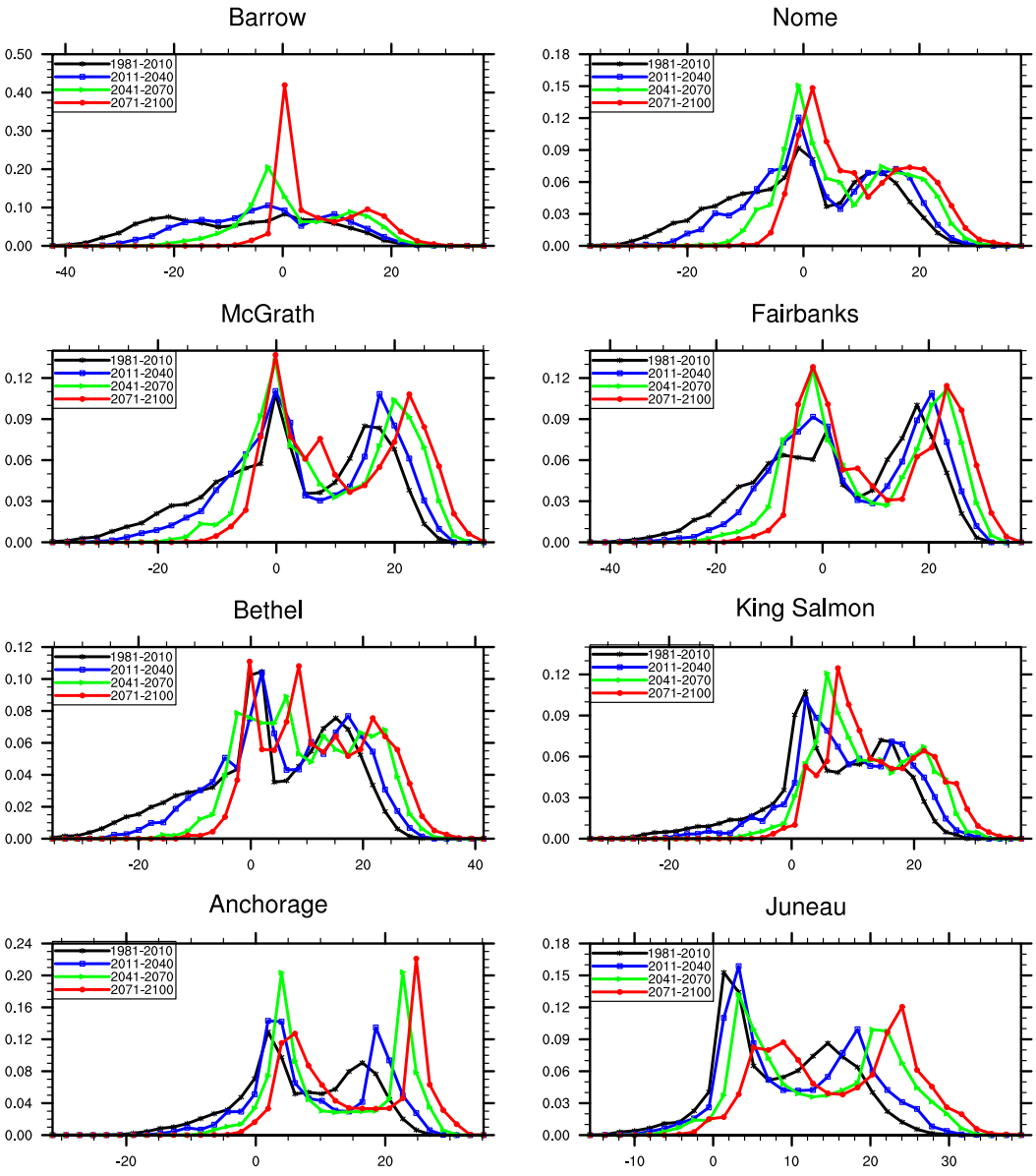

FIG. 7. Probability density function of daily T_{max} for the nearest downscaled grid cell to selected cities in Alaska for 1981–2010 (black), 2011–40 (blue), 2041–70 (green), and 2071–2100 (red).

3. Projections of extreme climate for Alaska during the twenty-first century

a. Temperature

Threshold-based indices of daily T_{max} and T_{min} suggest a further shrinking of the traditional cold season in Alaska and an increase in unprecedented summer heat. The annual number of icing days (ID), those with a daily T_{max} below 0°C, is projected to decrease 38% by 2100 statewide (Table 1). Its counterpart for daily T_{min}, the annual number of frost days (FD; $T_{min} < 0$°C), shows an average decrease of over two months statewide (Fig. 5). Meanwhile, the annual count of days with a high temperature above 25°C, so-called "summer days" (SU), is expected to skyrocket from a historical statewide average of 1.5 days yr^{-1} up to 29.7 days yr^{-1} (Fig. 6). Similarly, the annual count of tropical nights (TR; $T_{min} >$ 20°C) transitions from a negligible number to a statewide average of 6.8 occurrences per year (Table 1). To date, this magnitude of heat has largely been restricted to interior Alaska, but end-of-century projections indicate an expansion to cover nearly all of the state.

The maximum seasonal value of daily T_{max} (TX_x), when averaged across Alaska over 30-yr periods, shows

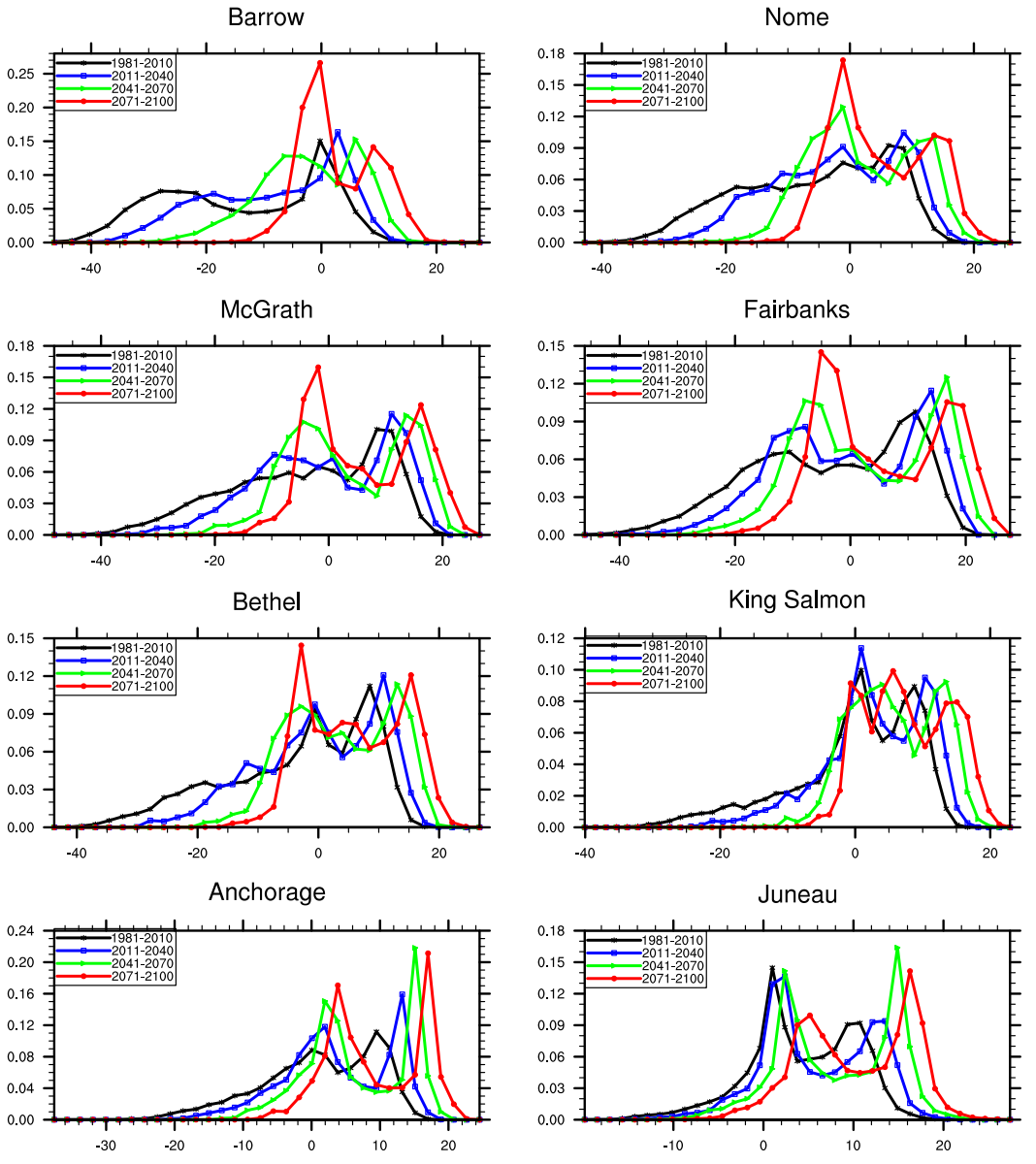

FIG. 8. As in Fig. 7, but for daily T_{min}.

projected increases of 6.2°, 7.5°, 7.0°, and 7.7°C for DJF, MAM, JJA, and SON, respectively, by 2100. For the monthly minimum value of daily T_{min} (TN_n), these increases are 18.2°, 16.3°, 6.8°, and 14.9°C, respectively. Thus, all seasons except summer indicate a much greater warming of extreme cold over extreme warm temperatures. The changes for TX_x and TN_n are approximately 50% and 25% larger, respectively, than those presented by Bennett and Walsh (2015), who used a 6-member ensemble of high-performing CMIP5 models for Alaska. This further suggests that the GFDL CM3 projects a stronger warming than the CMIP5 ensemble mean.

The asymmetric warming of cold extremes relative to warm extremes is apparent in the probability density functions of daily T_{max} (Fig. 7) and T_{min} (Fig. 8) at the nearest grid point to eight primary population centers of Alaska (Fig. 1). The 8-city average of the 30-yr minimum temperature increases by 22°C from 1981–2010 to 2071–2100 for both distributions of daily T_{max} and T_{min}. At the lower quartile, the magnitude of change decreases to approximately half that of the absolute minima, and the least change occurs at the upper quartile and the absolute maxima of the distributions (Table 2). Notable is the bimodality of many of these distributions, often representing cold- and warm-season modes. With

TABLE 2. The minimum (Min), lower quartile (Q1), median (Med), upper quartile (Q3), maximum (Max), and standard deviation (SD) of daily T_{max} (°C), and T_{min} (°C) for successive 30-yr periods for the nearest downscaled grid cell to selected cities in Alaska.

Station		T_{max} (°C)						T_{min} (°C)					
		Min	Q1	Med	Q3	Max	SD	Min	Q1	Med	Q3	Max	SD
Barrow	1981–2010	−43.9	−20.3	−7.1	4.0	27.1	14.3	−48.0	−25.7	−13.1	−0.4	16.6	13.7
	2011–40	−39.4	−12.2	−2.9	7.3	29.2	12.1	−43.3	−18.0	−6.1	2.0	19.6	11.6
	2041–70	−29.5	−3.9	−0.2	10.7	30.3	9.5	−34.4	−8.0	−2.0	5.3	19.8	8.6
	2071–2100	−15.7	0.1	2.9	13.6	34.9	7.8	−23.4	−2.0	0.4	8.5	25.0	6.4
Nome	1981–2010	−38.0	−8.8	0.4	11.0	28.8	12.6	−44.0	−15.3	−3.9	4.7	17.6	11.9
	2011–40	−29.3	−4.5	1.8	13.3	32.4	11.2	−35.6	−9.9	−1.3	6.9	20.6	10.2
	2041–70	−21.9	−1.1	5.4	15.7	34.1	9.9	−28.4	−4.5	0.8	9.6	24.1	8.3
	2071–2100	−11.8	1.2	8.0	17.8	36.6	9.3	−18.0	−1.7	3.5	11.9	24.5	7.6
McGrath	1981–2010	−39.1	−6.1	1.9	14.9	28.1	13.3	−49.5	−13.7	−2.2	8.0	19.3	13.2
	2011–40	−31.7	−3.1	3.5	17.2	29.7	12.2	−41.0	−9.5	−0.4	10.4	19.6	11.6
	2041–70	−25.2	−0.7	7.5	20.0	32.1	11.3	−33.1	−5.0	2.0	13.1	22.4	10.1
	2071–2100	−16.3	1.0	10.0	21.8	34.8	10.8	−25.7	−2.4	4.6	14.9	25.1	9.3
Fairbanks	1981–2010	−45.2	−7.9	2.5	16.5	30.5	14.4	−47.4	−14.3	−2.5	8.7	22.5	13.6
	2011–40	−39.0	−5.0	3.6	18.9	29.9	13.4	−43.0	−10.5	−0.6	11.4	21.0	12.3
	2041–70	−30.5	−2.5	7.0	21.3	31.8	12.8	−36.0	−6.9	1.5	14.0	23.1	11.4
	2071–2100	−24.7	−0.7	9.7	23.2	36.8	12.4	−27.2	−3.9	3.6	16.0	26.2	10.7
Bethel	1981–2010	−36.4	−3.7	2.9	14.2	30.5	12.4	−44.9	−11.7	−0.8	7.0	17.7	12.0
	2011–40	−25.5	−0.9	6.0	16.3	32.4	11.2	−32.3	−6.7	0.7	9.1	19.6	10.0
	2041–70	−16.7	1.4	8.7	18.8	34.9	10.1	−24.3	−3.3	3.3	11.5	21.7	8.5
	2071–2100	−11.9	4.0	10.8	20.7	39.3	9.7	−19.6	−1.7	5.5	13.5	24.8	8.1
King Salmon	1981–2010	−33.8	1.1	6.8	14.7	28.3	9.9	−40.9	−4.2	1.3	7.3	16.8	9.3
	2011–40	−21.2	3.1	8.9	16.5	30.4	8.8	−27.2	−1.1	2.9	9.3	18.8	7.6
	2041–70	−13.5	5.7	10.9	19.0	32.4	8.0	−18.2	1.0	5.3	11.7	20.3	6.3
	2071–2100	−5.9	7.6	12.6	20.6	36.5	7.9	−13.9	2.7	7.0	13.3	22.7	6.2
Anchorage	1981–2010	−32.4	1.1	6.3	15.2	27.4	9.2	−38.5	−4.3	1.7	8.5	17.7	8.5
	2011–40	−27.1	2.4	7.2	18.8	29.1	9.2	−33.0	−1.5	2.9	11.9	18.3	7.8
	2041–70	−21.0	3.9	10.4	22.2	32.2	9.5	−25.4	1.4	4.8	14.9	21.4	7.4
	2071–2100	−13.2	6.1	13.9	24.2	35.0	9.2	−17.5	3.7	7.6	16.6	23.5	6.8
Juneau	1981–2010	−16.6	2.3	7.8	14.9	31.7	7.6	−20.5	0.5	4.0	9.4	21.1	6.0
	2011–40	−13.9	3.1	9.3	17.7	33.2	8.3	−19.8	1.5	5.1	11.6	21.6	6.1
	2041–70	−9.9	4.9	13.4	21.4	36.6	9.1	−14.4	2.8	8.0	14.5	23.2	6.4
	2071–2100	−8.6	8.2	16.4	23.3	39.0	8.7	−12.8	5.1	10.2	16.0	26.6	6.1

time, extreme cold values warm and populate the bin near freezing, which results in peaky behavior. Despite the warming, Alaska will continue to experience polar night and ice-covered surfaces during winter, which could constrain the temperature to near freezing. The summer mode shifts more uniformly to the right.

The observed interannual variability, quantified by standard deviation, decreases at all stations except for Anchorage (T_{max}) and Juneau, Alaska (both T_{max} and T_{min}). This points to the importance of sea ice and seasonally permanent snowpack as drivers of extreme cold and high temperature variability. Anchorage and Juneau are much less affected by these drivers in the base period of 1981–2010 than are the other six stations. However, for the other locations proximal to where seasonal sea ice currently exists, sea ice and the presence of long-standing snowpack are projected to diminish by the midcentury and disappear entirely by 2100. As a stark consequence of this, Barrow, Alaska (now known as Utqiaġvik), which currently has high temperature variability similar to that of interior Alaska, exhibits comparable variability to Juneau by 2100 (Table 2).

b. *Precipitation*

Total precipitation is projected to increase across Alaska through time. The average annual accumulation increases from 79.3 cm yr^{-1} during the base period to 121.2 cm yr^{-1} by the end of the century, representing an increase of 53%. Note that these represent statewide averages; the Gulf of Alaska coast, including southeast Alaska and the Kenai Peninsula, typically have values exceeding 200 cm yr^{-1}, whereas the Arctic coast is often around 15–30 cm yr^{-1}. The changes to extreme precipitation are similarly striking. The average annual count of heavy precipitation days (R10; ≥10 mm) and very heavy precipitation days (R20; ≥20 mm) increases by 66% and 101%, respectively (Table 1). The average annual maximum 1- (Table 1) and 5-day (Fig. 9) precipitation is projected to increase by 53% and 50%, respectively, by the end of the century. The greatest

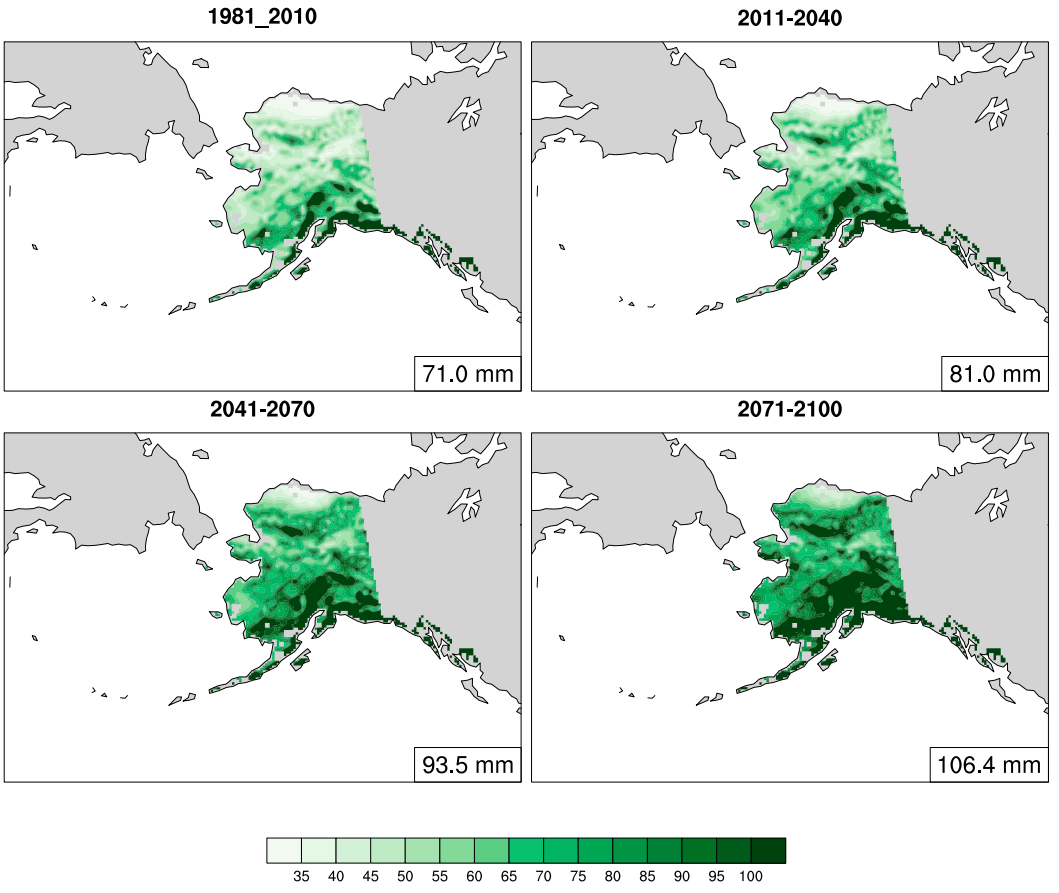

FIG. 9. Annual RX5 (mm) averaged for successive 30-yr periods. The statewide average is located at the bottom right.

relative change by percentage is expected for the Brooks Range and locations farther north. The average annual maximum number of consecutive wet days (CWD; ≥1.0 mm) is expected to increase by 23%, whereas the number of consecutive dry days (CDD) is projected to decrease by 21% (Table 1). This does not necessarily mean that the threat for severe drought would decrease, however, because higher temperatures would lead to greater daily evapotranspiration.

At the station (i.e., gridpoint) level, most locations are expected to see a median increase in daily precipitation, with each successive 30-yr period becoming wetter than the previous (Table 3). The exceptions to this are Juneau and Anchorage, which are projected to have comparable or even smaller median precipitation by 2100. The 90th and 99th percentiles of the 30-yr distributions are projected to increase at all stations through time. The absolute maximum precipitation amount does not necessarily increase with each period, but the end-century quantities are larger than those from the base period in all cases.

There is also an apparent connection between diminishing sea ice and extreme precipitation across western Alaska. The average daily sea ice extent during March, when the climatological maximum annual extent is reached, extends well south in the Bering Sea to between St. Paul Island and the Aleutian Islands from 2011 to 2040, but this line recedes into the Chukchi Sea from 2071 to 2100 (Fig. 10). Coincident with these losses of sea ice is an increasing trend for greater extreme precipitation, first for the Aleutian Islands and southwest Alaska from 2041 to 2070 and then for the Bering Strait and northwest Alaska from 2071 to 2100 (Table 3). Possible mechanisms for this relationship include shifting storm tracks and dynamics along the ice edge and greater local evaporation in areas where sea ice has been replaced by open water (Kopec et al. 2016).

4. Discussion

The observed and expected changes to extreme climate in Alaska show similarities but also some marked

TABLE 3. The Med, 90th percentile (90P), 99th percentile (99P), Max, and annual total of daily precipitation (mm) averaged over successive 30-yr periods for the nearest downscaled grid cell to selected cities in Alaska.

Station		Precipitation (mm)				
		Med	90P	99P	Max	Annual
Barrow	1981–2010	0.07	1.73	6.99	24.62	217.72
	2011–40	0.10	2.06	8.04	30.67	263.93
	2041–70	0.12	2.69	9.77	28.67	335.84
	2071–2100	0.19	3.58	12.28	34.68	439.88
Nome	1981–2010	0.06	4.66	17.47	43.43	541.55
	2011–40	0.12	5.61	21.10	48.52	661.58
	2041–70	0.15	7.02	25.23	62.91	825.44
	2071–2100	0.24	8.62	29.77	93.62	1022.17
McGrath	1981–2010	0.35	5.59	16.50	39.34	683.52
	2011–40	0.50	6.36	18.72	50.56	794.53
	2041–70	0.61	7.62	21.61	88.60	944.63
	2071–2100	0.65	7.82	25.02	90.53	1010.98
Fairbanks	1981–2010	0.18	4.02	13.62	45.37	495.86
	2011–40	0.21	4.62	16.39	68.76	582.42
	2041–70	0.26	5.48	18.80	97.92	696.25
	2071–2100	0.33	6.22	21.27	65.54	797.80
Bethel	1981–2010	0.31	5.68	15.63	44.18	670.10
	2011–40	0.37	6.02	17.66	50.09	740.51
	2041–70	0.55	7.16	20.41	76.77	879.44
	2071–2100	0.64	7.91	23.24	59.90	975.55
King Salmon	1981–2010	0.47	6.51	16.25	40.92	772.03
	2011–40	0.54	7.40	18.70	61.02	874.61
	2041–70	0.75	8.63	23.09	53.15	1050.73
	2071–2100	0.72	9.56	25.61	62.00	1139.54
Anchorage	1981–2010	0.21	5.79	18.49	65.77	686.93
	2011–40	0.21	6.77	22.25	54.11	796.59
	2041–70	0.19	7.42	25.09	64.39	879.51
	2071–2100	0.20	8.86	28.51	102.48	1024.03
Juneau	1981–2010	1.37	14.18	32.88	92.07	1747.05
	2011–40	1.25	15.16	35.72	144.02	1816.60
	2041–70	0.86	16.77	41.80	137.88	1963.05
	2071–2100	1.16	20.54	47.72	163.74	2353.02

differences when compared with the contiguous United States. For example, the asymmetric shift in the distributions of daily T_{max} and T_{min} is evident beyond Alaska; Meehl et al. (2016) show that for the continental United States, there has been an observed 2:1 ratio of record high maximum to record low minimum temperatures set during the early part of the twenty-first century. A similar analysis for Alaska shows that this ratio routinely exceeds 3:1 beginning in the 1990s and even climbs to 9:1 for the recent warm year of 2015 (Fig. 11). The circulation pattern likely contributed to the extreme warmth of 2014 and 2015, which saw both El Niño and strongly positive PDO conditions. These years are not included in the reference period used for mapping and thus do not affect the projections. However, they highlight how background warming in combination with favorable large-scale teleconnection patterns, which may or may not be captured well in the climate model, can result in extraordinary climate extremes.

The frost-free period in the eastern two-thirds of the contiguous United States is projected to increase by 30–40 days by 2100 (Walsh et al. 2014), whereas for Alaska, the statewide average increase of the growing season length (GSL) in this study is nearly 50 days (Table 1). Whether or not this increased growing potential is realized will largely depend on soil conditions and precipitation.

The average statewide precipitation distribution for Alaska is projected to increase nearly uniformly in a percentage sense; annual mean precipitation and maximum 1-day precipitation (RX1) are both expected to increase by 53%. The most extreme precipitation in the contiguous United States is expected to increase by smaller amounts of approximately 10%–40%, depending on season, and mean precipitation is even projected to decrease in parts of the central and southern United States (Prein et al. 2016). Furthermore, the annual maximum number of consecutive dry days is projected to increase across most of the contiguous United States (Walsh et al. 2014) but is expected to decrease by 21% in Alaska (Table 1).

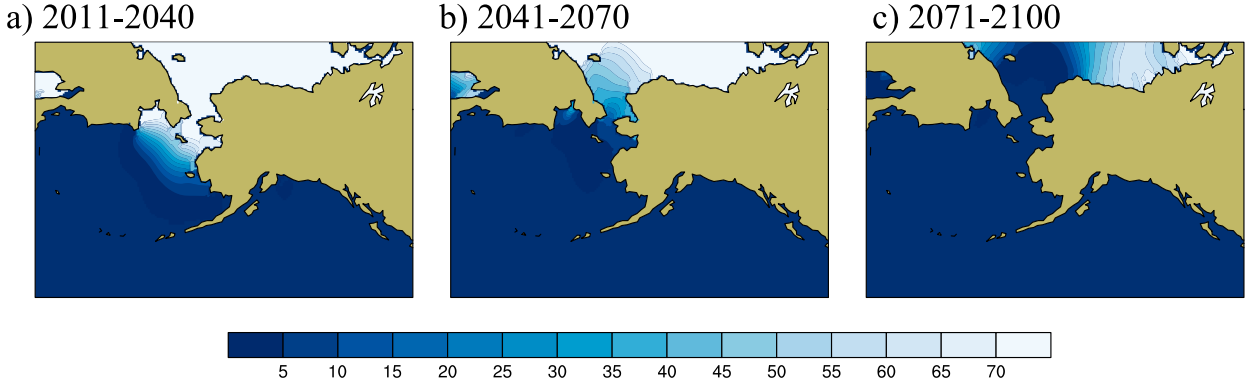

FIG. 10. Average daily sea ice concentration (%) during March for (a) 2011–40, (b) 2041–70, and (c) 2071–2100.

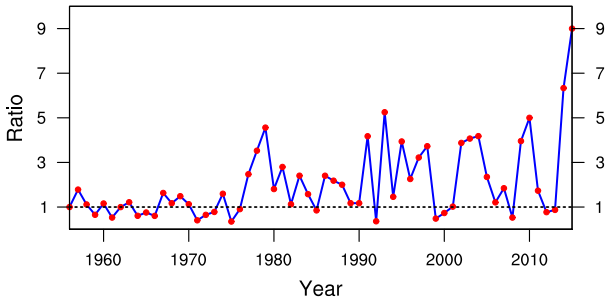

FIG. 11. Ratio of record high to record low temperatures for an aggregate of eight cities across Alaska from 1956 to 2015 (blue line). This is based on daily station observations of T_{max} and T_{min} from Anchorage, Barrow, Bethel, Fairbanks, Juneau, King Salmon, McGrath, and Nome. The expected ratio (dashed black line) assumes no change in extreme temperatures.

In terms of Clausius–Clapeyron scaling, the average surface specific humidity is projected to increase 5.7% $(°C)^{-1}$ statewide and 6.4% $(°C)^{-1}$ for the 99th percentile. For temperature–precipitation scaling, these values are 4.1% and 5.8% $(°C)^{-1}$, respectively. These values represent changes between 2071–2100 and 1981–2010. The 5.7% $(°C)^{-1}$ rate exactly matches the differential rate of change found by O'Gorman and Muller (2010), where it is suggested that scaling is lower than the expected 6%–7% $(°C)^{-1}$ because of slight decreases in relative humidity over land. The upper-percentile values are closer to expected Clausius–Clapeyron scaling possibly because they represent instances of high moisture transport and convergence.

For a signal-to-noise analysis of the extremes indices, the change signal can be represented by the 10-yr running mean anomaly relative to the historical GFDL CM3 and the noise by the interannual standard deviation of the same period. A signal-to-noise ratio of two indicates that the decadal mean is twice the historical standard deviation, indicating that a change signal is emergent. For the annual frost days index, the ratio

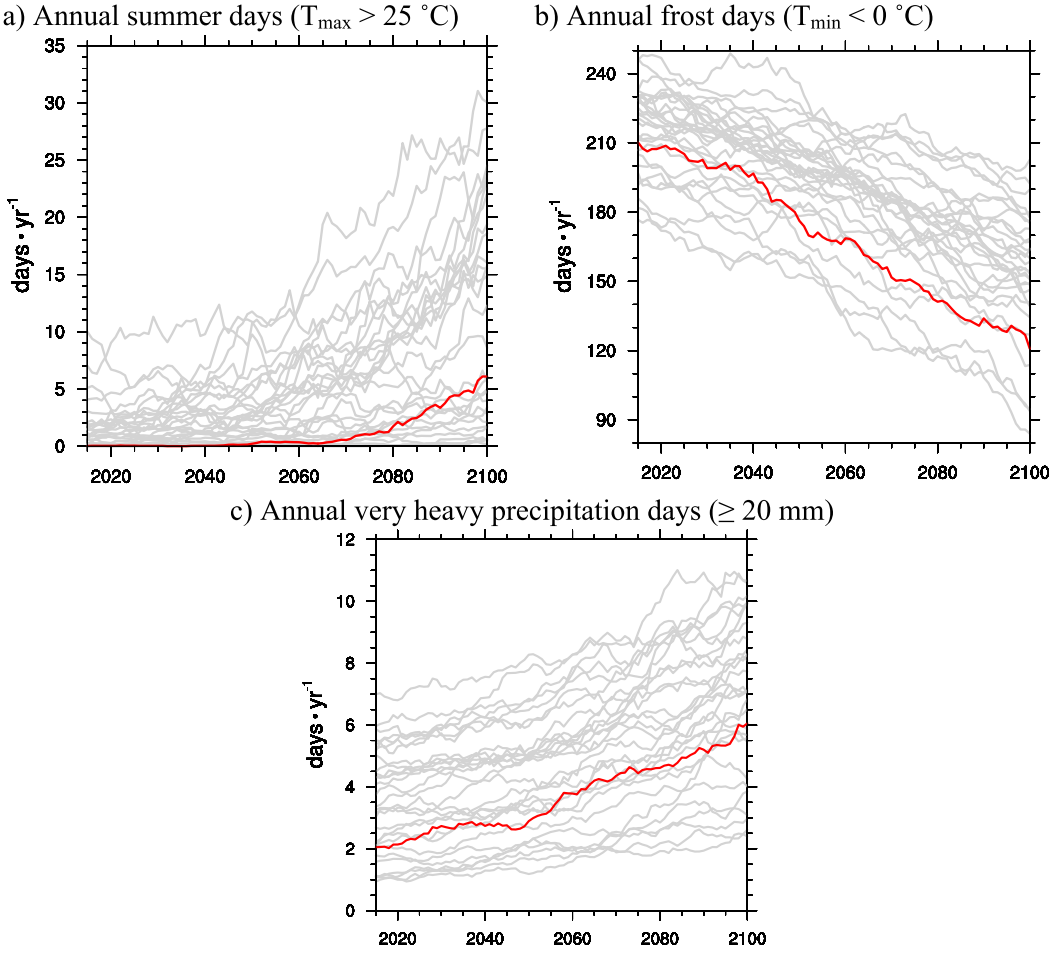

FIG. 12. Annual statewide 10-yr running mean of (a) SU (T_{max} > 25°C), (b) FD (T_{min} < 0°C), and (c) R20 (≥20 mm) from 30 CMIP5 RCP8.5 models. These represent the forcing data used for subsequent downscaling and here have been regridded to the WRF grid. The GFDL CM3 is indicated (red line).

continuously exceeds two from 2026 onward and for the annual maximum consecutive 5-day precipitation (RX5) from 2043 onward. However, no signal emerges for consecutive wet or dry days through 2100 (Table 1). This suggests that for indices with emergence dates before midcentury, the current level of change is already (or is close to) producing new extremes behavior. However, for indices with emergence dates after midcentury (e.g., tropical nights), the choice of emissions scenario could significantly change their future state. The use of a 10-yr running mean anomaly here is designed to provide a robust estimate of signal emergence that accounts for interannual variability. The signal emergence dates shown in Table 1 represent a statewide average and are likely to vary considerably by location.

Despite being a warm and wet model for Alaska relative to the CMIP5 RCP8.5 ensemble mean, indices of several extremes computed from the GFDL CM3 output generally fall near the middle of the range of projections from 29 other models (Fig. 12). These data were interpolated to the WRF grid, calculated for the Alaska land cells, and chosen to represent each of the meteorological variables in this study—summer days (T_{max}), frost days (T_{min}), and very heavy precipitation days (precipitation). This suggests that, while the downscaling effect can be large, use of different models in this study would likely not offer drastically different results. Global files for each of these models containing the Climate Indices of Extremes (CLIMDEX) indices are available from the Canadian Centre for Climate Modeling and Analysis (http://climate-modelling.canada.ca/climatemodeldata/climdex/).

5. Conclusions

This study investigates multiple dynamically downscaled datasets for Alaska to demonstrate that extreme daily temperatures (T_{max} and T_{min}) are projected to warm asymmetrically, with cold extremes warming the fastest. Total precipitation is expected to increase statewide, largely because of more intense precipitation, and with higher relative changes north of the Brooks Range. The percentage increase in short-duration heavy precipitation amounts is greater than for the contiguous 48 states (Walsh et al. 2014). The combination of these findings suggests that unprecedented heat and precipitation would occur throughout Alaska and that freezing temperatures and frozen precipitation would become increasingly less frequent by late century. These changes would favor increased plant productivity and an increased growing season length but would likely also increase the risk for severe fire years, warm-season flash flooding, and landslides. The exact timing of the most drastic changes is in part a function of when sea ice vanishes entirely, particularly for the Arctic coast; however, the overall signal of the magnitude of change is clear.

The downscaling products in this study are shown to better reflect observations of temperature than are the original coarse input data during the historical period, indicating a value-added response as a result of higher resolution. The GFDL CM3 RCP8.5 future scenario, which is warmer and wetter than the CMIP5 ensemble means, tracks better with recent trends in Arctic sea ice and near-surface temperatures, and without meaningful diversion away from the current trajectory of greenhouse gas emissions, it remains highly plausible. This future scenario was also bias adjusted to the downscaled ERA-Interim using quantile-delta mapping to further reduce errors. The bias adjustments of the entire distributions represent a value-added contribution to the evaluation of changes in extremes of temperature and precipitation for Alaska.

Acknowledgments. Support for this work was provided by the National Science Foundation Office of Polar Programs through Grant PLR-1268350 and by the NOAA Climate Program Office through Grant NA16OAR4310162 to the Alaska Center for Climate Assessment and Policy. This work was also made possible through financial support from the Alaska Climate Science Center, funded by the Cooperative Agreement G10AC00588 from the U.S. Geological Survey. Its contents are solely the responsibility of the author and do not necessarily represent the official view of the USGS. We thank three anonymous reviewers and the editor for providing excellent suggestions for how to improve our manuscript.

REFERENCES

Bekryaev, R. V., I. V. Polyakov, and V. A. Alexeev, 2010: Role of polar amplification in long-term surface air temperature variations and modern Arctic warming. *J. Climate*, **23**, 3888–3906, doi:10.1175/2010JCLI3297.1.

Bennett, K. E., and J. E. Walsh, 2015: Spatial and temporal changes in indices of extreme precipitation and temperature for Alaska. *Int. J. Climatol.*, **35**, 1434–1452, doi:10.1002/joc.4067.

Bieniek, P. A., J. E. Walsh, R. L. Thoman, and U. S. Bhatt, 2014: Using climate divisions to analyze variations and trends in Alaska temperature and precipitation. *J. Climate*, **27**, 2800–2818, doi:10.1175/JCLI-D-13-00342.1.

——, U. S. Bhatt, J. E. Walsh, T. S. Rupp, J. Zhang, J. R. Krieger, and R. Lader, 2016: Dynamical downscaling of ERA-Interim temperature and precipitation for Alaska. *J. Appl. Meteor. Climatol.*, **55**, 635–654, doi:10.1175/JAMC-D-15-0153.1.

Cannon, A. J., S. R. Sobie, and T. Q. Murdock, 2015: Bias correction of GCM precipitation by quantile mapping: How well do methods preserve changes in quantiles and extremes? *J. Climate*, **28**, 6938–6959, doi:10.1175/JCLI-D-14-00754.1.

Chapin, F. S., III, S. F. Trainor, P. Cochran, H. Huntington, C. Markon, M. McCammon, A. D. McGuire, and M. Serreze, 2014: Alaska. *Climate Change Impacts in the United States: The Third National Climate Assessment*, J. M. Melillo, T. C. Richmond, and G. W. Yohe, Eds., U.S. Global Change Research Program, 514–536, doi:10.7930/J00Z7150.

Dee, D. P., and Coauthors, 2011: The ERA-Interim reanalysis: Configuration and performance of the data assimilation system. *Quart. J. Roy. Meteor. Soc.*, **137**, 553–597, doi:10.1002/qj.828.

Donner, L. J., and Coauthors, 2011: The dynamical core, physical parameterizations, and basic simulation characteristics of the atmospheric component AM3 of the GFDL global coupled model CM3. *J. Climate*, **24**, 3484–3519, doi:10.1175/2011JCLI3955.1.

Giorgi, F., C. Jones, and G. R. Asnar, 2009: Addressing climate information needs at the regional level: The CORDEX framework. *WMO Bull.*, **58**, 175–183.

Glisan, J. M., and W. J. Gutowski Jr., 2014a: WRF summer extreme daily precipitation over the CORDEX Arctic. *J. Geophys. Res. Atmos.*, **119**, 1720–1732, doi:10.1002/2013JD020697.

——, and ——, 2014b: WRF winter extreme daily precipitation over the North American CORDEX Arctic. *J. Geophys. Res. Atmos.*, **119**, 10 738–10 748, doi:10.1002/2014JD021676

Groisman, P. Ya., R. W. Knight, D. R. Easterling, T. R. Karl, G. C. Hegerl, and V. N. Razuvaev, 2005: Trends in intense precipitation in the climate record. *J. Climate*, **18**, 1326–1350, doi:10.1175/JCLI3339.1.

Hayhoe, K. A., 2010: A standardized framework for evaluating the skill of regional climate downscaling techniques. Ph.D. dissertation, University of Illinois at Urbana–Champaign, 158 pp. [Available online at http://www.snap.uaf.edu/attachments/1_Hayhoe_Katharine.pdf.]

Hill, D. F., N. Bruhis, S. E. Calos, A. Arendt, and J. Beamer, 2015: Spatial and temporal variability of freshwater discharge into the Gulf of Alaska. *J. Geophys. Res. Oceans*, **120**, 634–646, doi:10.1002/2014JC010395.

Iacono, M. J., J. S. Delamere, E. J. Mlawer, M. W. Shephard, S. A. Clough, and W. D. Collins, 2008: Radiative forcing by long-lived greenhouse gases: Calculations with the AER radiative transfer models. *J. Geophys. Res.*, **113**, D13103, doi:10.1029/2008JD009944.

IPCC, 2012: *Managing the Risks of Extreme Events and Disasters to Advance Climate Change Adaptation.* C. B. Field et al., Eds., Cambridge University Press, 582 pp.

Janjić, Z., 1994: The step-mountain eta coordinate model: Further developments of the convection, viscous sublayer, and turbulence closure schemes. *Mon. Wea. Rev.*, **122**, 927–945, doi:10.1175/1520-0493(1994)122<0927:TSMECM>2.0.CO;2.

Klein Tank, A. M. G., F. W. Zwiers, and X. Zhang, 2009: Guidelines on analysis of extremes in a changing climate in support of informed decisions for adaptation. WMO Tech. Doc. WMO-TD 1500, 56 pp. [Available online at http://www.wmo.int/datastat/documents/WCDMP_72_TD_1500_en_1_1.pdf.]

Koenigk, T., P. Berg, and R. Döscher, 2015: Arctic climate change in an ensemble of regional CORDEX simulations. *Polar Res.*, **34**, 24 603, doi:10.3402/polar.v34.24603.

Kopec, B. G., X. Feng, F. A. Michel, and E. S. Posmentier, 2016: Influence of sea ice on Arctic precipitation. *Proc. Natl. Acad. Sci. USA*, **113**, 46–51, doi:10.1073/pnas.1504633113.

Lader, R., U. S. Bhatt, J. E. Walsh, T. S. Rupp, and P. A. Bieniek, 2016: Two-meter temperature and precipitation from atmospheric reanalysis evaluated for Alaska. *J. Appl. Meteor. Climatol.*, **55**, 901–922, doi:10.1175/JAMC-D-15-0162.1.

Laliberté, F., S. E. L. Howell, and P. J. Kushner, 2016: Regional variability of a projected sea ice-free Arctic during the summer months. *Geophys. Res. Lett.*, **43**, 256–263, doi:10.1002/2015GL066855.

Meehl, G. A., C. Tebaldi, and D. Adams-Smith, 2016: US daily temperature records past, present, and future. *Proc. Natl. Acad. Sci. USA*, **113**, 13 977–13 982, doi:10.1073/pnas.1606117113.

Morrison, H. C., G. Thompson, and V. Tatarskii, 2009: Impact of cloud microphysics on the development of trailing stratiform precipitation in a simulated squall line: Comparison of one- and two-moment schemes. *Mon. Wea. Rev.*, **137**, 991–1007, doi:10.1175/2008MWR2556.1.

NCEI, 2017: Climate at a glance: U.S. time series. NESDIS, accessed 13 April 2017. [Available online at http://www.ncdc.noaa.gov/cag/.]

O'Gorman, P. A., and C. J. Muller, 2010: How closely do changes in surface and column water vapor follow Clausius–Clapeyron scaling in climate change simulations? *Environ. Res. Lett.*, **5**, 025207, doi:10.1088/1748-9326/5/2/025207.

Overland, J. E., M. Wang, J. E. Walsh, and J. C. Stroeve, 2014: Future Arctic climate changes: Adaptation and mitigation time scales. *Earth's Future*, **2**, 68–74, doi:10.1002/2013EF000162.

——, E. Hanna, I. Hanssen-Bauer, S.-J. Kim, J. E. Walsh, M. Wang, U. S. Bhatt, and R. L. Thoman, 2016a: Surface air temperature. NOAA. [Available online at http://www.arctic.noaa.gov/Report-Card/Report-Card-2016/ArtMID/5022/ArticleID/271/Surface-Air-Temperature.]

——, ——, ——, ——, ——, ——, ——, and ——, 2016b: Air temperature [in "State of the Climate in 2015"]. *Bull. Amer. Meteor. Soc.*, **97** (8), S132–S134.

Parkinson, C. L., 2014: Global sea ice coverage from satellite data: Annual cycle and 35-yr trends. *J. Climate*, **27**, 9377–9382, doi:10.1175/JCLI-D-14-00605.1.

Partain, J. L., Jr., and Coauthors, 2016: An assessment of the role of anthropogenic climate change in the Alaska fire season of 2015 [in "Explaining Extremes of 2015 from a Climate Perspective"]. *Bull. Amer. Meteor. Soc.*, **97** (12), S14–S18, doi:10.1175/BAMS-D-16-0149.1.

Peters, G. P., and Coauthors, 2013: The challenge to keep global warming below 2°C. *Nat. Climate Change*, **3**, 4–6, doi:10.1038/nclimate1783.

Pithan, F., and T. Mauritsen, 2014: Arctic amplification dominated by temperature feedbacks in contemporary climate models. *Nat. Geosci.*, **7**, 181–184, doi:10.1038/ngeo2071.

Prein, A. F., R. M. Rasmussen, K. Ikeda, C. Liu, M. P. Clark, and G. J. Holland, 2016: The future intensification of hourly precipitation extremes. *Nat. Climate Change*, **6**, 48–52, doi:10.1038/nclimate3168.

Riahi, K., and Coauthors, 2011: RCP 8.5—A scenario of comparatively high greenhouse gas emissions. *Climatic Change*, **109**, 33–57, doi:10.1007/s10584-011-0149-y.

Sillmann, J., V. V. Kharin, X. Zhang, F. W. Zwiers, and D. Bronaugh, 2013a: Climate extremes indices in the CMIP5 multimodel ensemble: Part 1. Model evaluation in the present climate. *J. Geophys. Res. Atmos.*, **118**, 1716–1733, doi:10.1002/jgrd.50203.

——, ——, F. W. Zwiers, X. Zhang, and D. Bronaugh, 2013b: Climate extremes indices in the CMIP5 multimodel ensemble: Part 2. Future climate projections. *J. Geophys. Res. Atmos.*, **118**, 2473–2493, doi:10.1002/jgrd.50188.

Skamarock, W. C., and Coauthors, 2008: A description of the Advanced Research WRF version 3. NCAR Tech. Note NCAR/TN-475+STR, 113 pp., doi:10.1056/D68S4MVH.

U.S. Environmental Protection Agency, 2016. Climate change indicators in the United States 2016. U.S. Environmental Protection Agency Rep. EPA 430-R-16-004, 96 pp. [Available online at http://www.epa.gov/climate-indicators.]

van Vuuren, D. P., and Coauthors, 2011: The representative concentration pathways: An overview. *Climatic Change*, **109**, 5–31, doi:10.1007/s10584-011-0148-z.

Walsh, J. E., and Coauthors, 2014: Our changing climate. *Climate Change Impacts in the United States: The Third National Climate Assessment*, J. M. Melillo, T. C. Richmond, and G. W. Yohe, Eds., U.S. Global Change Research Program, 19–67, doi:10.7930/J0KW5CXT.

——, P. Bieniek, B. Brettschneider, E. Euskirchen, R. Lader, and R. Thoman, 2017: The exceptionally warm winter of 2015/16 in Alaska. *J. Climate*, **30**, 2069–2088, doi:10.1175/JCLI-D-16-0473.1.

Zhang, J., U. S. Bhatt, W. V. Tangborn, and C. S. Lingle, 2007: Climate downscaling for estimating glacier mass balances in northwestern North America: Validation with a USGS benchmark glacier. *Geophys. Res. Lett.*, **34**, L21505, doi:10.1029/2007GL031139.

Zhang, X., and J. Zhang, 2001: Heat and freshwater budgets and pathways in the Arctic Mediterranean in a coupled ocean/sea-ice model. *J. Oceanogr.*, **57**, 207–237, doi:10.1023/A:1011147309004.

——, L. Alexander, G. C. Hegerl, P. Jones, A. Klein Tank, T. C. Peterson, B. Trewin, and F. W. Zwiers, 2011: Indices for monitoring changes in extremes based on daily temperature and precipitation data. *Wiley Interdiscip. Rev.: Climate Change*, **2**, 851–870, doi:10.1002/wcc.147.